Check for updates

Received: 23 December 2019 | Revised: 7 February 2020 | Accepted: 28 March 2020

DOI: 10.1002/jemt.23494

RESEARCH ARTICLE

MICROSCOPY RESEARCH & TECHNIQUE WILEY

Morphological analysis of aqueous humor drainage using QD nanoparticles and indocyanine green

İsmail Hakkı Nur[1] | Şerife Saçmacı[2] | İmdat Orhan[1] | William Perez[3] | Haluk Testereci[4]

[1]Department of Anatomy, Faculty of Veterinary Medicine, Erciyes University, Kayseri, Turkey

[2]Department of Chemistry, Science Faculty, Erciyes University, Kayseri, Turkey

[3]Área de Anatomía, Facultad de Veterinaria, Universidad de la República, Montevideo, Uruguay

[4]Department of Medical Biochemistry, Faculty of Medicine, Karadeniz Technical University, Trabzon, Turkey

Correspondence
İsmail Hakkı Nur, Department of Anatomy, Faculty of Veterinary Medicine, Erciyes University, Kayseri, Turkey.
Email: hn63@erciyes.edu.tr; hnur_55@hotmail.com

Funding information
Erciyes Üniversitesi, Grant/Award Number: TOA-2017-7362

Abstract

This study represents the first morphological description of the lymphatic drainage of the ciliary body in vivo by comparative hyperspectral fluorescence imaging techniques of Quantum Qdot655 (QD) nanoparticles and indocyanine green (ICG). A volume of 1.25 μl of QD was injected into the left anterior camera of all rats. Similarly,1.25 μl of ICG diluted at a ratio of one-fourth with physiological saline solution was injected into the right anterior camera of all rats. The thickness of the skin in the mandibular area, connective tissue, and the depth of the mandibular lymph node (MLN) made image retrieval difficult. For QD, 302 nm UV excitation and 605 nm fluorescence peak emission were applied. The detection of QD and ICG used in this study in the MLNs is definitive evidence that aqueous humor (AH) follows a uveolymphatic pathway. Scanning electron microscope and the energy dispersive X-ray analyzer spectrum were used to examine both the Schlemm's canal and the MLN. For the first time, the QD was detected in the cortex of MLN. The QCM analysis of both QD-AH and ICG-AH was used to determine whether there was any interaction between them. This comparative study shows the importance of experimental animal modeling in pharmacological studies regarding eye research and drugs. In a female rat, the signal was taken from the parotid lymph node with QD injections.

KEYWORDS

in vivo imaging, indocyanine green, lymphatic drainage, quantum dot655, Schlemm's canal

1 | INTRODUCTION

Nontoxic substances such as indocyanine green (ICG) have been used for a long time in the diagnosis of various diseases of the eye. Recently, Quantum dots (QD) have been used in biological research because of their bright fluorescence, adjustable fluorescence signal, narrow emission spectrum, wide UV excitation, and greater photostability. ICG has a peak spectral absorption at about 800 nm. The wavelength of near-infrared (NIR) light is approximately 700 ~ 1,000 nm. This range is the least absorbed by blood or water. ICG has a half-life of 150 to 180 seconds. It operates in the NIR, in which tissues are much more translucent than in visual (Ishizawa, Saiura, & Kokudo, 2016) wavelengths. QD also has a peak spectral absorption at 655 nm.

Drainage of aqueous humor (AH) out of the eye occurs in two ways. These are conventional outflow and uveoscleral outflow (UVS). In the conventional outflow pathway, the AH passes through the trabecular meshwork (TM) and exits the eye. AH is drained from the TM into the Schlemm's canal (SC). SC is a collector channel system. It connects the episcleral venous system to the bloodstream. In the unconventional (UVS) outflow pathway, AH passes from the base of the iris (iridocorneal angle formed by the iris and cornea) from the interstitial tissue within the ciliary corpus to the suprachoroidal space. The AH suprachoroidal space then exits the sclera through loose connective tissue around the blood vessels and the sclera itself (Figure 1).

There are numerous published articles describing the structure of the eye and its adaptation to the surrounding environmental

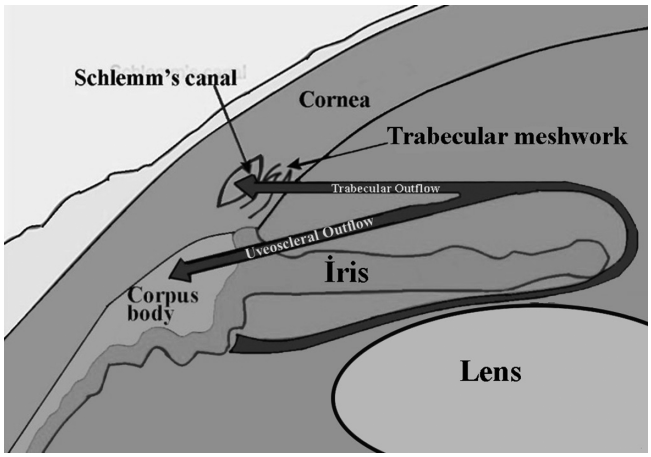


FIGURE 1 Aqueous humor (AH) outflow pathway
The AH exits the anterior chamber via two main outflow pathways. A fraction of AH flows through the trabecular meshwork located at the anterior chamber angle. The AH then enters the juxtacanalicular tissue and inner wall endothelium of Schlemm's canal and subsequently drains into the episcleral veins. This outflow pathway is called the trabecular or conventional outflow. The other second pathway is the uveoscleral outflow pathway. The remaining AH leaves the anterior chamber through the intercellular spaces of the iris root, ciliary muscle, sclera, and eventually empties into the episcleral tissues. This outflow pathway is generally known as the uveoscleral or unconventional outflow [Color figure can be viewed at wileyonlinelibrary.com]

conditions (Nur & Güler, 2002). However, by 2040, the number of blind people due to glaucoma will have reached up to 120 million. Glaucoma is treated by the removal of intraocular pressure (IOP). Glaucoma is the leading cause of irreversible blindness in the world (Raychaudhuri, Millar, & Clark, 2018). In 2010, there were an estimated 60.5 million people across the globe with primary open-angle glaucoma or primary angle-closure glaucoma, and this number is projected to increase up to 111.8 million by 2040 (Kingman, 2004; Quigley & Broman, 2006; Tham et al., 2014; Wong, Loon, & Saw, 2006). The increasing prevalence of glaucoma can affect an individual's health, relating to the quality of life, and continues to have significant economic burdens (Varma, Lee, Goldberg, & Kotak, 2011). Therefore, the treatment of patients with glaucoma is crucial. Glaucoma is characterized by elevated IOP which is related to progressive vision loss.

The ultimate therapeutic goal in patients with glaucoma is the successful control of IOP. IOP can be controlled through medical therapy or surgical management. However, glaucoma has not still been sufficiently controlled with the current therapies. Therefore, new pathways and agents are needed for the treatment of glaucoma (Schlotzer Schrehardt, 2007). AH is drained from the eye via two main pathways: conventional outflow through the TM and SC; and unconventional outflow through the ciliary body. Both pathways are well studied (Gobel, Rufer, & Erb, 2011; Swaminathan, Oh, Kang, & Rhee, 2014; Tamm, Braunger, & Fuchshofer, 2015). The third pathway for AH drainage was described by Yücel et al. (2009). This newly discovered route is the "uveolymphatic" pathway in the ciliary body.

Recent studies using various markers have revealed the presence of the lymphatic drainage in the eyes of humans, sheep, and mice. It is known that the circulation of lymph fluid originates from lymphoid tissues (Kim, Johnston, Gupta, Moore, & Yucel, 2011; Tam, Gupta, Zhang, & Yucel, 2011; Yucel, 2010; Yücel et al., 2009; Yucel & Gupta, 2015). The optical clarity is crucial for the vision. For this reason, excess protein must be removed from the eye. However, it is not clear how these are separated from the eye.

The lymphatic system has a well-established role in the drainage of extracellular fluid and solutes in most organs. Lymphatic vessels are highly permeable to macromolecules, many proteins, and migrating cells, and transport them to the lymph nodes and then into the blood circulation (Alitalo, Tammela, & Petrova, 2005; Chachaj & Szuba, 2013; Huggenberger et al., 2010; Jafarnejad, Woodruff, Zawieja, Carroll, & Moore Jr., 2015). As was previously revealed, the lymphatic drainage is absent or nonfunctional in the eye (Bill, 1975). However, the recently published data confirmed that the lymphatic drainage of the eye appeared to be active. When the various tracers were injected into the eye, their drainage channels were identified using immunofluorescence (Yücel et al., 2009). Recently available in vivo imaging of QD can be used for screening of the lymphatic tissues (Nur, Sacmaci, Keles, Abumandour, & Testereci, 2019; Tam et al., 2011; Yucel & Gupta, 2015).

There are morphological descriptions of the lymphatic drainage of the eye, especially using in vivo imaging of QD in Wistar albino rats. Therefore, the current work was prepared to give a full morphological evaluation of the lymphatic drainage of the eye, using an in vivo hyperspectral fluorescence imaging techniques of QD nanoparticles and ICG.

2 | MATERIALS AND METHODS

2.1 | Collection of animal samples

Sixteen female and sixteen male 8-week-old Wistar albino rats weighing 250–300 g were obtained from the animal research center called DEKAM at the Erciyes University (ERU). Both sexes were rats at the beginning of their reproductive stage. It was also aimed to determine whether gender has an effect on signals. The rats were kept at room temperature in cages under continuous 12-hour light/dark cycles and fed ad libitum with standard food and water before and during the experiments. This study was approved on March 15, 2017, with the code 171026 by the Committee for the Ethics of Animal Research (ERUHADYEK) at the University of Erciyes-Kayseri-Turkey, and the required ethics guidelines were followed.

2.2 | Anesthesia procedure

General anesthesia was induced by the intraperitoneal route. For this purpose, 0.3 ml (0.6 ml xylazine, 0.24 ml ketamine) was used for the males, while 0.2 ml (0.6 ml xylazine, 0.14 ml ketamine) was used for the females (Nur et al., 2019).

TABLE 1 Intraocular pressure (IOP) for left and right eyes of male and female rats, amount of given indocyanine green (ICG) and Quantum dot (QD) levels and related observed images from the submandibular lymph node were given in the 15th and 40th minutes, the 6th and 10th hours after injection

	IOP (mmHg) (left/right eye)		Amount of ICG (μl) right eye		Amount of Qdot (μl) left eye		The image in the submandibular lymph node															
							ICG								QD							
Rat no	M	F	M	F	M	F	15 min (M)	15 min (F)	40 min (M)	40 min (F)	6th hr (M)	6th hr (F)	10th hr (M)	10th hr (F)	15 min (M)	15 min (F)	40 min (M)	40 min (F)	6th hr (M)	6th hr (F)	10th hr (M)	10th hr (F)
1	26/24	21/20	1.25	1.25	1.25	1.25	–	–	–	–	–	+	*	*	–	–	–	–	–	–	*-	*
2	24/24	17/18	1.25	1.25	1.25	1.25	–	–	–	–	–	+	*	*	–	–	–	–	–	+	–(•)	+(•)
3	26/27	20/21	1.25	1.25	1.25	1.25	–	–	–	–	+	–	*	*	–	–	–	–	–	–	*	*
4	23/24	16/17	1.25	1.25	1.25	1.25	–	–	–	–	+	+	*	*	–	–	–	–	–	–	*	*
5	26/26	26/27	1.25	1.25	1.25	1.25	–	–	–	–	–	+	+(•)	+(•)	–	–	–	–	–	–	*	*
6	16/15	14/15	1.25	1.25	1.25	1.25	–	–	–	+	+	+	*	*	–	–	–	–	+	–	*	*
7	18/19	26/24	1.25	1.25	1.25	1.25	–	–	–	–	+	–	–	*	–	–	–	–	–	–	–(•)	+(•)
8	24/26	26/30	1.25	1.25	1.25	1.25	–	–	+	–	+	–	*	*	–	–	+	–	+	–	*	*
9	24/26	25/29	1.25	1.25	1.25	1.25	–	–	–	–	–	+	*	*	–	–	–	–	+	+	*	*
10	18/17	20/23	1.25	1.25	1.25	1.25	–	–	–	–	–	+	–(•)	+(•)	–	–	–	–	–	–	*	*
11	15/15	20/21	1.25	1.25	1.25	1.25	–	–		–	+	+	*	*	–	–	–	–	+	–	*	*
12	17/17	24/25	1.25	1.25	1.25	1.25	–	–	–	–	+	+	*	*	–	–	–	+	–	+	*	*
13	19/17	26/26	1.25	1.25	1.25	1.25	–	–	–	–	+	–	*	*	–	–	+	–	+	–	–(•)	+(•)
14	14/13	28/29	1.25	1.25	1.25	1.25	–	–	–	–	+	+	*	*	–	–	–	+	+	–	*	*
15	17/16	22/24	1.25	1.25	1.25	1.25	–	–	–	–	+	+	*	*	–	–	–	–	–	–	–(•)	+(•)
16	17/15	27/27	1.25	1.25	1.25	1.25	–	–	+	–	+	–	*	*	–	–	–	–	–	–	*	*

Note: (•) Signs depict the images of some of the randomly-selected rats at the 10th hour. For ICG. Rat No: 5, 10. For Qdot 655. Rat No.: 2, 7, 13, and 15.

*: No measurement, –: No signal observed, +: Signal observed.

2.3 | Anterior camera injection of QD and ICG as the tracer

In this study, Qdot655 and ICG were used as a comparative study. The absorption of the ICG reagent in tissues was negligible and also a stronger signal could be used.

The hair on the head, neck, front of the chest, and forelimb areas of the rats were shaved down by hair trimmer (Moser 1871 Chromstyle, Germany). After hair removal process, 1.25 μl of QD (8 μM solution in a 50 mM borate buffer; Invitrogen, Eugene, Oregon) was injected into the anterior chamber of the left eyes on all rats using the Hamilton syringe with 33-gauge needle (Hamilton Company, Reno, Nevada) under a dissection microscope (Olympus SZ-PT, Tokyo, Japan). Similarly, 1.25 μl of ICG diluted at a ratio of one-fourth with physiological saline solution was injected into the right camera oculi anterior of all rats. The left eyes of all rats received QD and soon after that, the right eyes received ICG.

2.4 | Measurement of IOP

In order to ensure moisture of the eyes for in vivo imaging, three drops of artificial eye drop were applied topically 17 hours before the attempt (n = 32) and 1 hour just before the experiment. IOP was measured by the application of Alcian (0.5% Sterile Ophthalmic Solution; active reagent: 5 mg Propalaine–HCl in 1 ml) which was added dropwise to each eye. Immediately after Alcian drops, IOP was measured in both eyes with a handled rebound tonometer (Tonolab, Type TV02; Icare Finland Oy, Helsinki, Finland) under general anesthesia.

2.5 | In vivo hyperspectral fluorescence imaging

Thirty-two Wistar albino rats were used for in vivo hyperspectral fluorescence imaging. Following 3–4 minutes of control measurements on the IOP, the anesthesia was repeated only during the imaging sessions at various time points such as prior to tracer injection, and at 15, 40, and 360 minutes after injection. No abnormal behavior was observed due to anesthesia. The tunable filter was automatically stepped in 10-nm increments from 500 to 800 nm, with an exposure time of 900 milliseconds. For ICG, 780 nm NIR excitation and 820 nm NIR emission filters were applied. The ICG emission is between 720 and 820 nm. Similarly, for QD, 302 nm UV excitation and 655 nm emission were used. Our Syngene system has Epi-NIR, Epi-UV, and Epi-RGB excitation sources and also all emission filters. In addition to these, six rats were selected randomly from both sexes and then in vivo fluorescence images were taken at the 10th hour (Nur et al., 2019). The size of the experimental animals, the depth of the lymph node, the thickness of the connective tissue and skin were the obstacles in obtaining proper fluorescent images.

For in vivo imaging, Syngene GBOX-XRQ (Cambridge, UK) device was used. A 655 nm emission filter for QD and LY800 nm filter for ICG were used to obtain those images. The Syngene tools' software program was used to process the images and retrieve the necessary reports.

2.6 | Scanning electron microscope

The rats were sacrificed under general anesthesia. In order to examine them under the electron microscope, the upper half of the body was separated from the lower half of the body, and the bulbus oculi of the rats were extracted under the dissection microscope (Olympus SZ-PT). Two round pieces, like a skullcap, were extracted from the cornea and at the optic nerve level under the dissecting microscope. The lens was carefully removed from the window. The collected samples were fixed in the solution (4% formaldehyde, 2.5% glutaraldehyde in 0.1 M sodium cacodylate buffer, pH 7.4) at 4°C for 48 hours. Then, these samples were put in the washing solution formed from 0.1 M sodium cacodylate containing 5% sucrose, processed by tannic acid. Later, the samples were dehydrated in increasing concentrations of ethanol (15 minutes in 50, 70, 80, 90, 95, and 100% ethanol). Final fixation was carried out in 1% osmium tetroxide followed by dehydration.

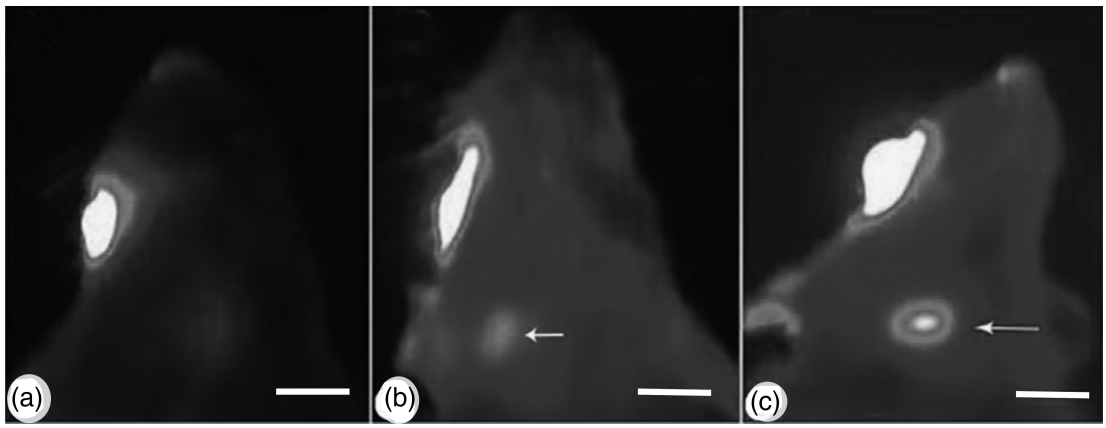


FIGURE 2 In vivo hyperspectral fluorescent images. On the right neck region, ventral view. The appearance of the hyperspectral fluorescence imaging on the right MLN of the female rats after the 15th minute (a), the 40th minute (b), and the 6th hour (c) following indocyanine green injection. The white arrow shows where the fluorescent signal appears and intensifies. Scale, 10 mm [Color figure can be viewed at wileyonlinelibrary.com]

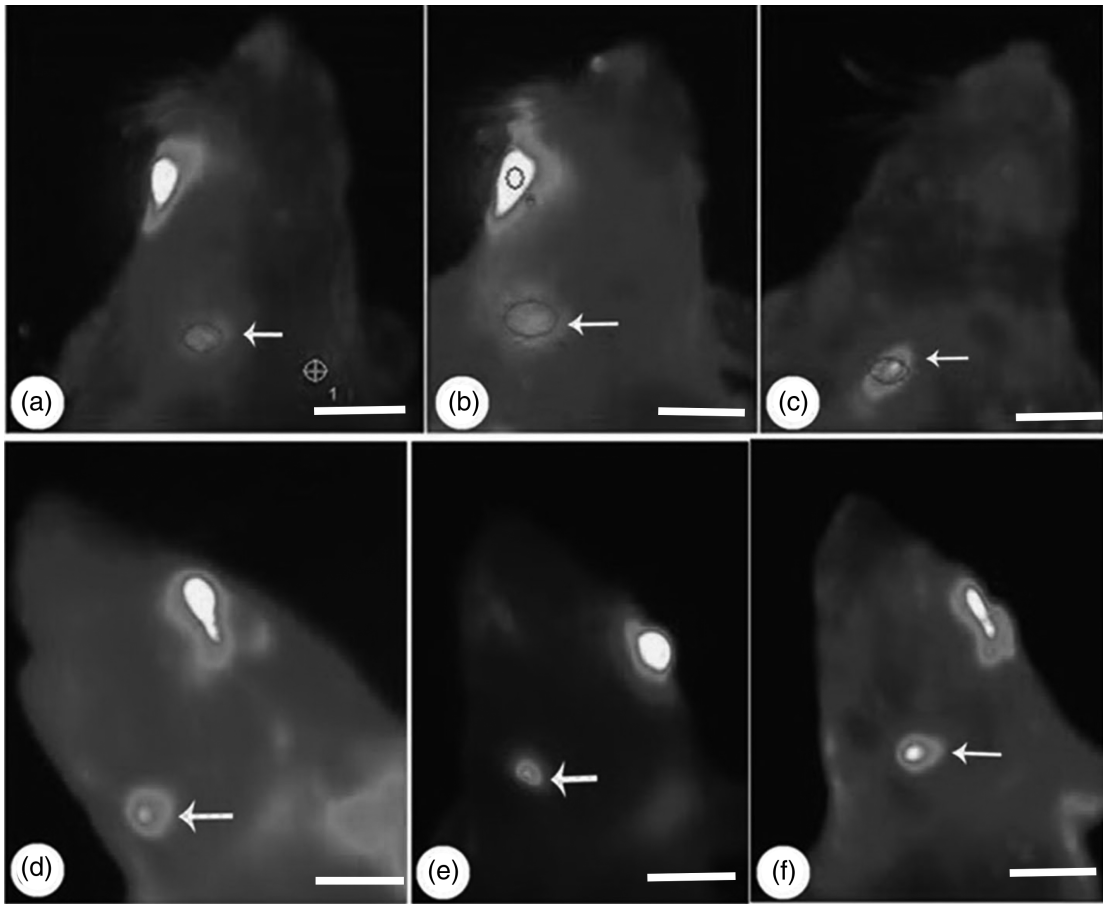


FIGURE 3 Comparison of in vivo hyperspectral fluorescent images after indocyanine green (ICG) and Quantum dots (QD) injections. On the right neck region (a–c), ventral view, and left neck region (d–f), lateral view
The upper three images (a–c) show fluorescence images in the right mandibular lymph node (MLN) for a male rat after receiving ICG injection into the right eye. The lower three images (d–f) show fluorescence images in the left MLN for a female rat after receiving QD injection to the left eye. The white arrow shows MLN where the fluorescent signal appears and intensifies. Timewise comparison of the signals on both sides of the MLN region of the neck. Images (a and d) taken at the 40th minute after related injections. Images (b and e) taken at the 6th hour after related injections. Images (c and f) taken at the 10th hour after related injections [Color figure can be viewed at wileyonlinelibrary.com]

After washing out excess fluids, the eyes were sliced in an anterior–posterior direction under a dissecting microscope. Finally, after the critical point drying, the samples were coated with gold–palladium in a sputtering device, and then they were scanned via a scanning electron microscope (SEM). Similar procedures were performed in the MLN. The tissues were examined under the dissecting microscope to determine their general anatomical features before the examination under the SEM. The specimens were observed and photographed under an SEM (ZEISS-EVO-LS-10) at 25 kV (Carl Zeiss, Inc., Thornwood, New York).

2.7 | Mapping with EDX spectrum on the electron microscope

EDX spectrum was used to observe nanoparticles at both SC and lymph node in order to demonstrate if there are any interactions between them. Using the EDX spectrum on SEM has created a great advantage and so far, it has not been used for this purpose previously. Similarly, mapping was performed to determine whether QD was retained in the MLN.

2.8 | Investigation of the presence of chemical or physical interaction with QCM-D (quartz crystal microarray)

Quartz crystal microarray (QCM) analysis reveals the physical or chemical interaction of two different fluids. Therefore, it was investigated whether QD and ICG interacted with AH. For this purpose, the QCM (Q-SenseE1 System, Sweden) was used. For QCM analysis, the gold surface of the instrument was coated with QD for 30 minutes at 4000 rpm by QD Spin Coater-Laurell Model WS-650-23, Laurell Technologies. For this purpose, 1.5 μl of AH from one male and one

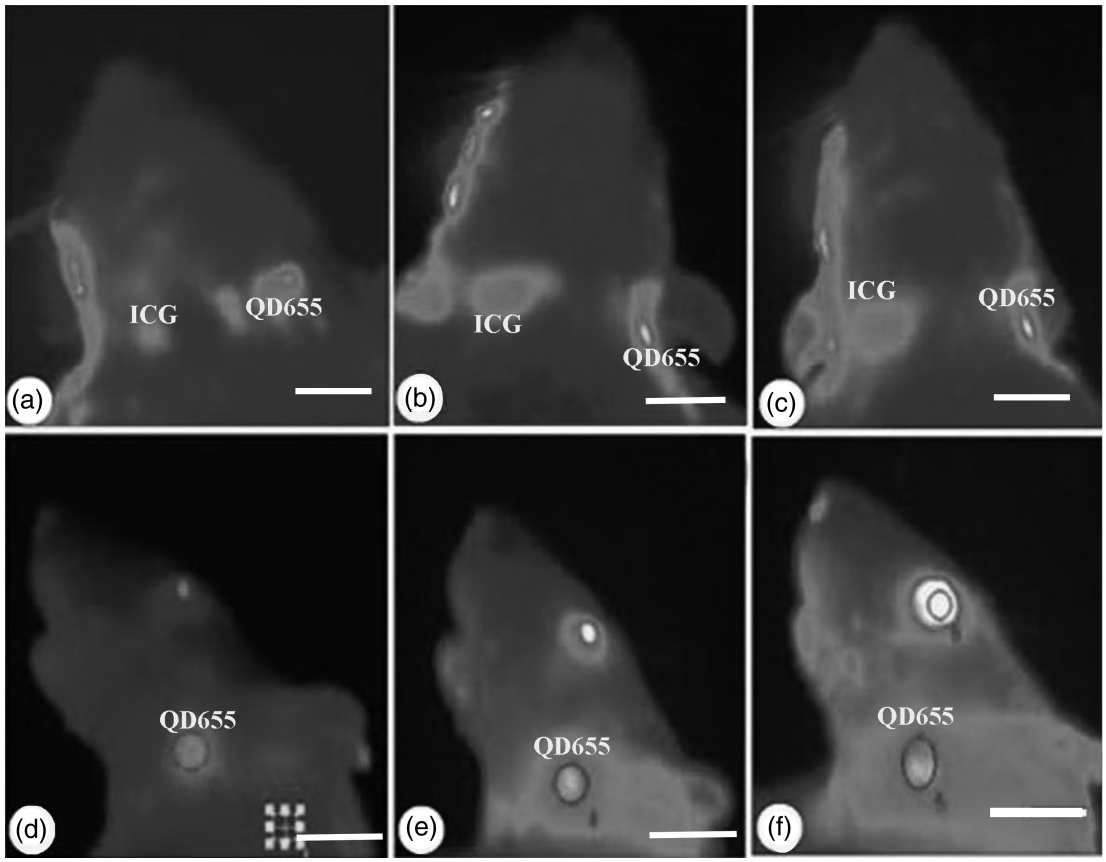


FIGURE 4 Comparison of in vivo hyperspectral fluorescent images after indocyanine green (ICG) and Quantum dots (QD) injections. On the right neck region (a–c), ventrodorsal view, and left neck region (d–f), lateral view.
Upper three images (a–c) demonstrate the appearance of fluorescence image at the mandibular lymph node (MLN) region after ICG and QD injections on a male rat. ICGs were initially injected into the left eye, whereas QD was injected into the right eye. QD fluorescence signals were observed at the 40th minute (a), the sixth hour (b), and the 10th hour (c) on the left MLN.
Lower three images (d–f) surprisingly demonstrate fluorescence imaging in the parotid lymph node region after QD injection of female rat grouped in five. Fluorescence images taken at left parotid lymph node received QD into the left eye were taken at the 15th and the 40th (e) minutes and the 6th (f) hour. Image f indicates that fluorescence emission of QD particles was widely scattered at the parotid region. Scale, 10 mm [Color figure can be viewed at wileyonlinelibrary.com]

female rat were obtained from their camera oculi anterior spaces, under general anesthesia. After that, 1.5 μl of AH fluid was mixed with 200 μl of ultra-distilled water. Later on, this mixture was passed through the sensor, via the tubing of the QCM device. QCM analyses had three variables: frequency, time, and dissipation: Frequency (Hz) in the graph shows the sensitivity of the electrical change on the sensor. Time (h: m: s) shows the measurement time. Dissipation indicates a mass spread or loss of coated liquid on the sensor. Frequency and dissipation are an inverse system.

3 | RESULTS

The results of the study were summarized in Table 1. After measuring each rat's IOP, QD was given to the left camera oculi anterior and ICG was given to the right camera oculi anterior. Fluorescence images were normally taken at the 15th, 40th, and 6th hours. However, additional six rats were randomly chosen among those to follow further fluorescence images at the 10th hour. While QD signals were tracked from the left side of the neck, ICG signals were tracked from the right side of the neck.

3.1 | In vivo hyperspectral imaging following anterior camera QD and ICG injection

No signal was detected within 15 minutes on both sides of the neck region after QD and ICG injections to both eyes (Figure 2a). As shown in Table 1, the fluorescence signals were observed in 3 rats after 40 minutes and 22 rats after 6 hours following ICG injections. Similarly, the fluorescence signals were observed in four rats after 40 minutes and nine rats after 6 hours following QD injection. When the follow-up time extended to 10th hour for QD injection, the four rats out of the randomly selected four female rats had shown some

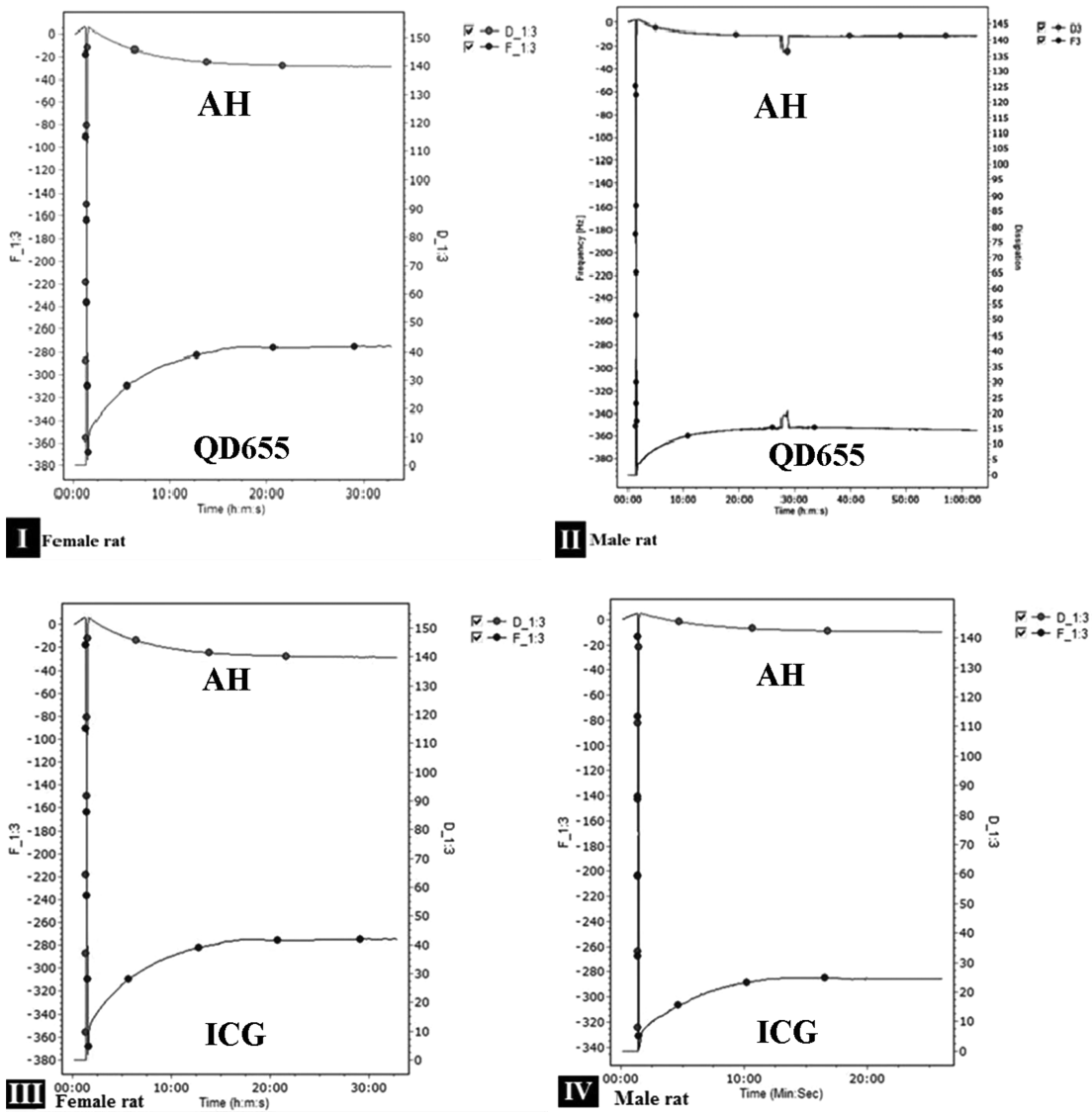


FIGURE 5 Interaction comparison among Quantum dots (QD)/aqueous humor (AH) (I and II) and indocyanine green (ICG)/AH (III and IV) was analyzed for both gender rats. The graphs show frequencies for ICG, QD, and AH vs time. The line above (red) is for AH, the black line below is for ICG. The blue line is for QD. These graphs show that both ICG and QD do not have a physical or chemical interaction with AH. 120 × 125mm (600 × 600 DPI) [Color figure can be viewed at wileyonlinelibrary.com]

signs. However, at the 10th hour following ICG injection, both of the two selected female rats had shown signals on the neck region.

3.2 | IOP values for both genders

The rats in the current experiments had a normal IOP level for both genders as shown in Table 1.

3.3 | In vivo ICG and QD images from MLNs at the 10th hour

The rats were chosen randomly and measurements from MLN were done at the 10th hour because the fluorescence power of QD was not either diffusing fast or images were not obtained clearly due to the size of the animal and skin thickness etc. Similar image problems existed for ICG measurements before the 10th hour as well, most especially dificulty in obtaining clear images from male rats prior to the 10th hour. Therefore, the proper start time for the measurements in MLN was selected as the 10th hour. The rat numbers and results are given in Table 1.

3.3.1 | Control measurements on the rats numbered as 5 and 10 for ICG

At the 10th hour as shown in Table 1, the female rat 5 had shown stronger signal than the male rat 5, but no signal was observed in male and female rats 10 (Figure 2b and c). In the first 40 minutes in male

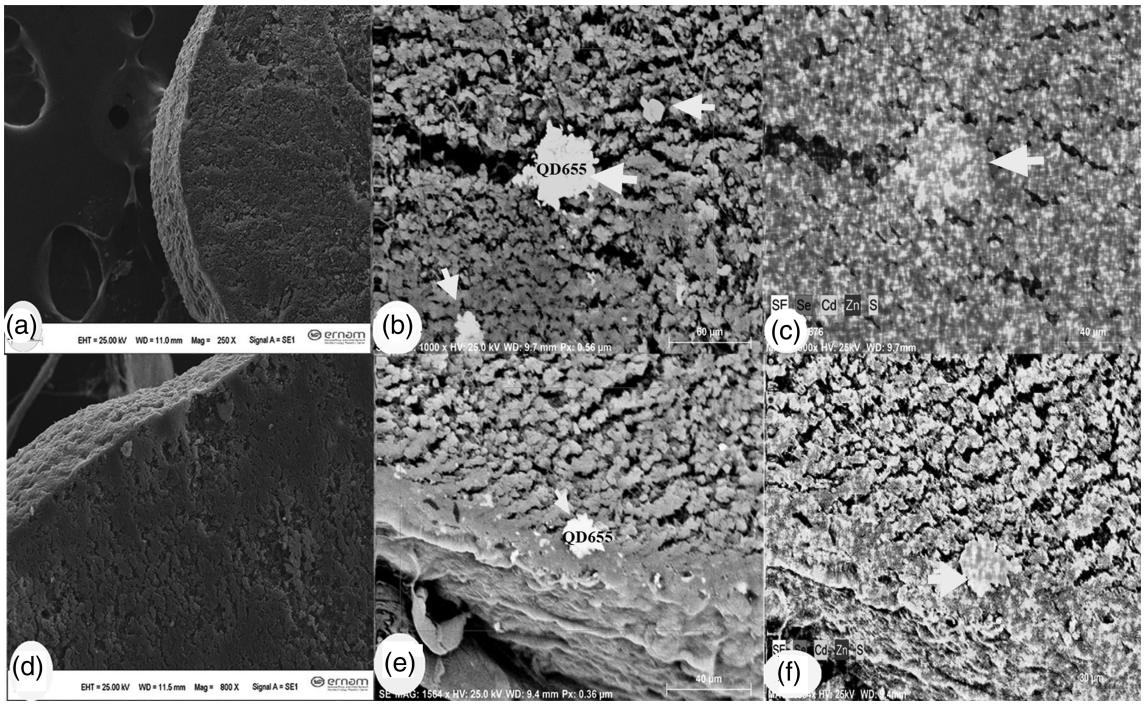


FIGURE 6 Cross-sections of the scanning electron microscope (SEM) image of the left mandibular lymph node (MLN) were given above. At the 6th hour following Quantum dots (QD) injection, (a–c) are for the male rat in Group 14 as well as and so are (d–f) are for the female rat in group 15. While (a) and (d) are nonmagnified SEM images, (b) and (c) are magnified (×1000) SEM images. (e) and (f) are also magnified (×1564) SEM images. The presence of QD has been indicated with a white arrow on view (b), (c), (e), and (d). Views (c) and (f) are for the energy dispersive X-ray analyzer spectrum that clearly indicated that given QD particles from camera oculi anterior reached MLN [Color figure can be viewed at wileyonlinelibrary.com]

rats (Figure 3a), almost no signal was received due to the location of MLN. When the time was further extended, the strength of the signals was increasingly obtained (Figure 3a–c).

3.3.2 | Control measurements on the rats numbered as 2, 7, 13, and 15 for QD

A closer look at Table 1 indicates that some images could be obtained at the 10th hour in some of the randomly selected rats, but not in others (Figure 3e and f). Meanwhile, the strongest signals were obtained in some other rats as shown in Figure 3f.The fluorescence signals were present in the female rats for all three observation time intervals (Figure 3d–f).

3.4 | Examples of images taken in rats for QD

While two male and two female rats had fluorescence images taken at the 40th minute, six male and two female rats had fluorescence images at the 6th hour following QD injection. When follow-up image taking time was extended to the 10th hour, four randomly selected female rats showed fluorescence images. Fluorescence images were not obtained in the MLN at the 40th minute in female rats injected with QD. The fluorescence images were weak at the sixth hour (Figure 3b and e). Fluorescence-intensified imaging could be obtained in the 10th-hour measurement (Figure 4c). It was thought that this was not due to the deep, subcutaneous connective tissue and the fat mass was not at the inhibitory level.

The number 2 female rat had almost no signal at the 40th minute (Figure 3d), and the fluorescent image was slightly poor in the sixth hour measurement. However, fluorescent imaging was found to be the strongest at the 10th hour (Figure 4a–c).

3.5 | Image of QD in the parotid lymph node

Although the fluorescence images at the 40th minute and at the 6th hour were detectable for the parotid region of female rat numbered 5, there was no fluorescence emission from male rat numbered 5. Variations on an image obtained in the parotid lymph node may be explained by the individual differences (Figure 4d–f).

3.6 | Using the QCM device for the determination of interaction on AH

The QCM analysis of both QD-AH and ICG-AH was used to determine whether there was any interaction between them (Figure 5). However, no interaction was detected between them.

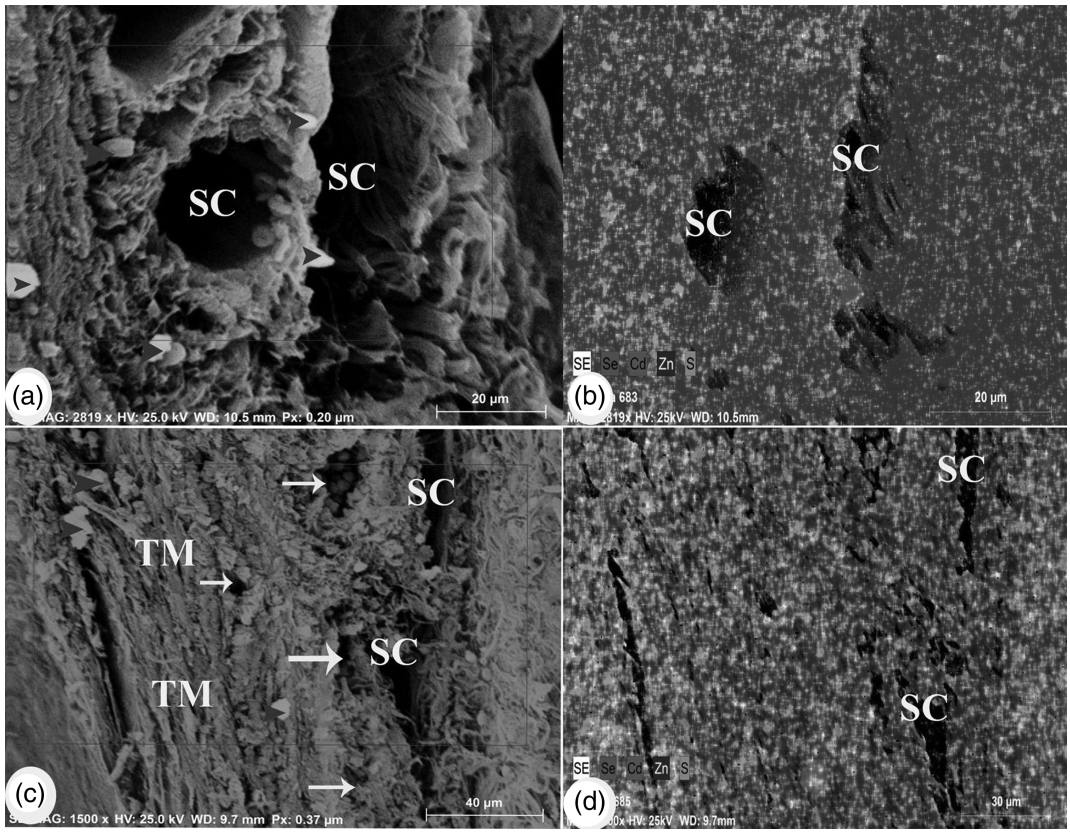


FIGURE 7 At the 6th hour, anteroposterior section of Schlemm's canal (SC) sections for the male rat in Group 4 are shown as a scanning electron microscope (SEM) image (a, ×2819) and energy dispersive X-ray analyzer (EDX) spectrum (b, ×2819) view above. At the same hour, anteroposterior sections of SC for the female rat in Group 9 are shown below as an SEM image (c, ×1500) and EDX spectrum (d, ×1500) view. The presence of Quantum dots was shown by the red arrow and arrowheads at the trabecular meshwork and SC on intertubercular spaces [Color figure can be viewed at wileyonlinelibrary.com]

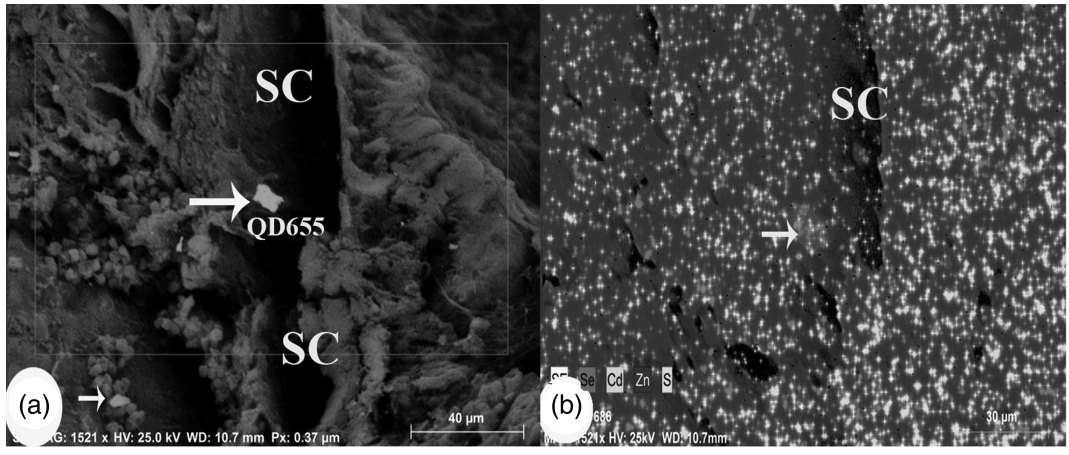


FIGURE 8 At the 6th hour, anteroposterior section of Schlemm's canal (SC) sections for the female rat in Group 14 are better shown as an scanning electron microscope image (a, ×1521) and energy dispersive X-ray analyzer spectrum (b, ×1521) view above. The presence of Quantum dots was shown by the white arrow at the SC on intertubercular spaces [Color figure can be viewed at wileyonlinelibrary.com]

3.7 | SEM analyses and results

Imaging of the morphology of the QD and ICG in the MLN was carried out. The SEM images were obtained from the right MLN for the ICG, from the left MLN for QD in both genders. The presence of QD in the right MLN was clearly demonstrated by SEM images (Figure 6). As described in Figure 7, the QD particles appeared as spherical particles on the surface of the MLN. In addition, they were not distributed homogeneously.

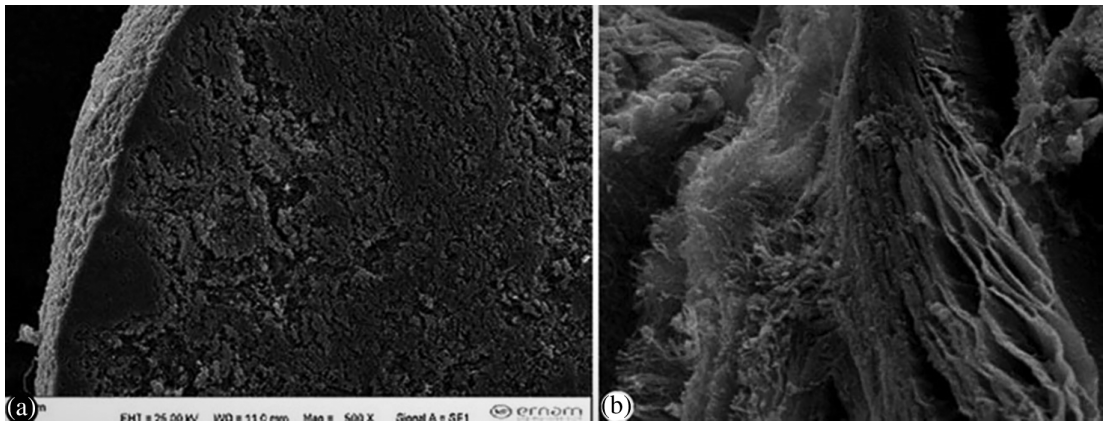


FIGURE 9 No indocyanine green fluorescence for all rats was observed as seen on the scanning electron microscope (SEM) image (a, ×500) of an anteroposterior section of the subcapsular, cortex, and medulla of the right mandibular lymph node and an SEM image (b, ×200) of an anteroposterior section of the right trabecular meshwork [Color figure can be viewed at wileyonlinelibrary.com]

3.8 | EDX analyses and results

The EDX spectra of the MLN were recorded (Figure 7c and f) in order to further confirm the surface modification of QD. The EDX spectrum of the MLN and QD showed the existence of zinc and sulfur, indicating the appropriate change and the presence of QD. SEM and EDX analyses images of the SC were recorded in male rat numbered 4 (Figure 7a and b), and female rat numbered 9 (Figure 7c and d), female rat numbered 14 (Figure 8). No data were obtained when the EDX spectrum of ICG was observed on the cross-section of the tissues (Figure 9).

4 | DISCUSSION

Understanding AH should be the cornerstone of understanding the pathogenesis of glaucoma and it will become an epidemic in the world in the coming decades (Tham et al., 2014). In addition, since TM and SC are the most important structures in this drainage route, most of the studies on this subject have focused on the drainage of the AH (Ferrer, 2006). Outflow pathways ensure stable IOP, although temporary IOP increases such as blinking and eye rubbing (Kim & Caprioli, 2018). According to this study, the mechanical changes in the TM ultrastructure will reduce the drainage of the AH. Also, mechanical changes will increase the deposition of the extracellular matrix material, altering the ultrastructure of the outflow pathway, and slowing down the drainage of the AH. This might be the reason why signals were obtained from only four rats within the first 60 minutes.

In our study, SEM displays nanoparticles for the first time both on the SC of the MLN with the EDX spectrum method. In addition to this, our study may be counted as unique since we detected for the first time, the presence of the cortex of MLN. However, its presence has been detected only in the subcapsular region of the MLN in a previously published article by Tam et al. (2011) using the immunofluorescence staining.

In the light of previous studies investigating the corrosion breakdown or drainage systems of the eye (Morrison, Fraunfelder, Milne, & Moore, 1995; Morrison, Johnson, Cepurna, & Funk, 1999; Ninomiya & Inomata, 2006), the consensus was that there was no lymphatic system in the eye (Gruntzig, Schicha, Kiem, Becker, & Feinendegen, 1978; Quigley & Broman, 2006). However, this opinion has lost its validity through the studies in recent years (Kim et al., 2011; Tam et al., 2011; Yücel et al., 2009). There has been an increasing interest in QD due to their hydrodynamic feature as they can penetrate into lymphatic vessels and lymph nodes and can also be used in in vivo imaging. Because this study shows the existence of QD in TM, it can be considered as the first example of its kind.

Detection of nanoparticles and ICG in MLN was examined in our study, which is clear evidence that AH follows an uveolymphatic route. However, experimental conditions such as the anatomical and physiological structures of the lymphatic system in the eye, general anesthesia, inactivity, and mechanical ventilation (Negrini & Moriondo, 2011) will lead to a remarkable decrease in the lymphatic flow. It was very difficult to get images from some rats in the first 40 minutes. In some of the rats, we hardly obtained images from some rats in the first 40 minutes, but we were able to obtain some clear images after the 10th hour due to the physiological differences or the pace of AH and/or the proper thickness of the skin and connective tissues. For that reason, as seen in Table 1, we obtained images of female rats easier than male rats.

We cannot rule out the possibility of releasing some QD earlier than the first detection period following the injection. This reduction in QD sensitivity may not be appropriate for the quantitative analysis of in vivo hyperspectral imaging (Rosenblum, Kosaka, Mitsunaga, Choyke, & Kobayashi, 2011). In the light of data that were obtained in this study, we can assert that QD and ICG, which were injected into the anterior camera, entered the lymphatic system, and reached the MLN. Also, the fluorescent microscopic data, electron microscopic and the in vivo images showed exactly the presence of uveolymphatic transition. This study may encourage further investigation of drug

effects on the eye's lymphatic output; it may also lead to new IOP lowering treatments. According to Crawford and Kaufman (1987), imaging of the lymphatic drainage in the eyes of sheep had the same obstacles as in our study. Although they could not obtain an in vivo image in their imaging system, they could only detect the presence of QDs in the dissected lymph nodes.

The presence of lymph vessels in the ciliary body of humans and other mammals is known. For this purpose, it has been noticed that radioactive materials injected into AH penetrated cervical lymphatics by protein markers. UVS drainage was estimated by measurement of tracer retained in uveal and scleral tissue harvested at the end of the experiments either 3 or 5 h after intracameral injection. A closer look at the ratios between trabecular drainage and uveoscleral drainage shows that they are different from each other. These ratios, in sheep, was 69:20, in Cynomolgus monkeys and Vervet monkeys (Bill, 1971) were 45:55 and 62:38, respectively, in mice (Aihara, Lindsey, & Weinreb, 2003), dogs (Barrie, Gum, Samuelson, & Gelatt, 1985) were 75:25 and 85:15, respectively. In rabbits and cats, its ratios were 92–97:3–8 and 97:3, respectively (Bill, 1966).

As known, prostanoids are used in the treatment of glaucoma and are known to enhance drainage from the UVS pathway. It was detected that they enhance UVS drainage by Prostaglandin F2 alpha and its derivatives in humans (Toris, Camras, & Yablonski, 1993) and monkeys (Nilsson, Sperber, & Bill, 1989), Prostaglandin D2 in rabbits (Goh, Araie, Nakajima, Azuma, & Hayaishi, 1989), and Prostaglandin A2 in cats (Toris, Yablonski, Wang, & Hayashi, 1995). Therefore, it is predicted that PGF2α treatment increases uveoscleral eye tissue (siliceous muscle) drainage and consequently increases lymphatic drainage. Lymphatic vessels respond to a wide range of biochemical and pharmacological agents. In addition, prostaglandin family appears to be especially important in regulating the active contractility of lymphatics, including prostaglandin analogs that enhance lymphatic drainage (Amann-Vesti, Gitzelmann, Koppensteiner, & Franzeck, 2003; Tam et al., 2011).

In our experimental study, signals obtained from the MLN 1–6 hours after injection of DQ and ICG into the anterior camera are shown in Table 1. In the light of data that were obtained in this study and literature, it was demonstrated that either QD or ICG that were injected into camera anterior entered the lymphatic system and reached mandibular lymph nodule. Also, both fluorescent microscopic data, electron microscopic and in vivo images showed exactly the presence of uveolymphatic transition. According to the findings of this study, it was observed that the QD had been drained toward the MLN. On the other hand, they were not seen in the cervical lymph nodes. The findings in our study, for the first time, show that QD injected into the anterior camera reached the parotid lymph node in the female rat. This was an important finding (Figure 4d–f).

AH's dynamics have been studied in various species as reported in the previously published data (Husain, Whitlock, Rice, & Crosson, 2006; Toris, Risma, Gonzales-Martinez, McLaughlin, & Dawson, 2010). In sheep, the trackers which are injected into the anterior camera are drained into the head and neck lymph nodes via the lymphatic system of the ciliary body. Some studies have shown that the antigens injected into the anterior camera may drain into the local lymph nodes (Kim et al., 2011). It can be argued that the tracer injected into the eye of the mouse partially reaches the MLN due to the fact that it is linked to the lymphatic system in the ciliary body (Yucel & Gupta, 2015). AH is drained through the UVS pathway; in addition to this way, it can be drained via the iris and uveolymphatic pathway. Further work is needed to determine the origin and portal of the lymph fluid that is drained via the orbital lymphatic system. It is very important to recognize the general pathways of MLN transfer from the anterior camera of QDs. It is possible that the lymphatic drainage of these tracers passes from the anterior chamber, through the most posterior aspects of the uveal meshwork, enters the open spaces between longitudinal aspects of the ciliary muscle, and then enters the suprachoroidal space.

This is the first comparative study on adult rats using ICG and QD. In addition, EDX analysis of both TM and MLN was performed to determine the presence of QD. In this aspect, this study is unique. In light of the data obtained in this study, images should be taken on computerized tomography to identify the route of the SC in laboratory animals. The mapping of SC should be demonstrated. Our study may be a guide for further studies.

5 | CONCLUSION

This study firstly revealed evidence of the lymphatic drainage in the eyes of Wistar albino rats. Lymphatic drainage in the eye was visualized in vivo by comparative hyperspectral fluorescence imaging techniques of QD and ICG. Ciliary body and sclera may play a role in AH drainage. Findings from this study support the use of this rat model as a potential source for future screening studies of drugs targeting ocular lymphatic drainage. Finally, defining the "Uveolymphatic" pathway, determining its structure and topographic mapping can give new ideas for reducing IOP in the treatment of glaucoma. On the other hand, biocompatible probes and more precise hyperspectral imaging methods need to be developed in order to determine the route of the drainage pathway between AH and MLN. In this way, new methods can be developed in the treatment of glaucoma and similar diseases that lead to blindness.

ACKNOWLEDGMENTS

The authors are grateful for the financial support provided by the Unit of Scientific Research Projects of Erciyes Üniversitesi (Project no: TOA-2017-7362).

CONFLICTS OF INTEREST

The authors declare no potential conflict of interest.

ORCID

İsmail Hakkı Nur https://orcid.org/0000-0001-7215-8112

REFERENCES

Aihara, M., Lindsey, J. D., & Weinreb, R. N. (2003). Aqueous humor dynamics in mice. *Investigative Ophthalmology & Visual Science*, *44*(12), 5168–5173. https://doi.org/10.1167/iovs.03-0504

Alitalo, K., Tammela, T., & Petrova, T. V. (2005). Lymphangiogenesis in development and human disease. *Nature*, *438*(7070), 946–953. https://doi.org/10.1038/nature04480

Amann-Vesti, B. R., Gitzelmann, G., Koppensteiner, R., & Franzeck, U. K. (2003). Isoprostane 8-epi-prostaglandin F2 alpha decreases lymph capillary pressure in patients with primary lymphedema. *Journal of Vascular Research*, *40*(1), 77–82. https://doi.org/10.1159/000068942

Barrie, K. P., Gum, G. G., Samuelson, D. A., & Gelatt, K. N. (1985). Quantitation of uveoscleraloutflow in normotensive and glaucomatous beagles by 3H-labeled dextran. *American Journal of Veterinary Research*, *46*(1), 84–88.

Bill, A. (1966). Formation and drainage of aqueous humour in cats. *Exp. Eye Res*, *5*, 185–190.

Bill, A. (1971). Aqueous humor dynamics in monkeys (Macaca irus and Cercopithecus ethiops). *Experimental Eye Research*, *11*(2), 195–206. https://doi.org/10.1016/s0014-4835(71)80023-4

Bill, A. (1975). Blood circulation and fluid dynamics in the eye. *Physiological Reviews*, *55*(3), 383–417. https://doi.org/10.1152/physrev.1975.55.3.383

Chachaj, A., & Szuba, A. (2013). Lymphatic endothelium. *Postepy Biochemii*, *59*(4), 379–385.

Crawford, K., & Kaufman, P. L. (1987). Pilocarpine antagonizes prostaglandin F2 alpha-induced ocularhypotension in monkeys. Evidence for enhancement of Uveoscleral outflow by prostaglandin F2 alpha. *Archives of Ophthalmology*, *105*(8), 1112–1116. https://doi.org/10.1001/archopht.1987.01060080114039

Ferrer, E. (2006). Trabecular meshwork as a new target for the treatment of glaucoma. *Drug News and Perspectives*, *19*(3), 151–158. https://doi.org/10.1358/dnp.2006.19.3.985929

Gobel, K., Rufer, F., & Erb, C. (2011). Physiology of aqueous humor formation, diurnal fluctuation of intraocular pressure and its significance for glaucoma. *Klinische Monatsblätter für Augenheilkunde*, *228*(2), 104–108. https://doi.org/10.1055/s-0029-1246040

Goh, Y., Araie, M., Nakajima, M., Azuma, I., & Hayaishi, O. (1989). Effect of topical prostaglandin D2 on the aqueous humor dynamics in rabbits. *Graefe's Archive for Clinical and Experimental Ophthalmology*, *227*(5), 476–481. https://doi.org/10.1007/bf02172902

Gruntzig, J., Schicha, H., Kiem, J., Becker, V., & Feinendegen, L. E. (1978). Studies on the lymph drainage of the eye 5. Quantitative registration of the lymph drainage from the subconjunctival space with a radioactive tracer (author's transl). *Klinische Monatsblätter für Augenheilkunde*, *172*(6), 872–876.

Huggenberger, R., Ullmann, S., Proulx, S. T., Pytowski, B., Alitalo, K., & Detmar, M. (2010). Stimulation of lymphangiogenesis via VEGFR-3 inhibits chronic skin inflammation. *The Journal of Experimental Medicine*, *207*(10), 2255–2269. https://doi.org/10.1084/jem.20100559

Husain, S., Whitlock, N. A., Rice, D. S., & Crosson, C. E. (2006). Effects of latanoprost on rodent intraocular pressure. *Experimental Eye Research*, *83*(6), 1453–1458. https://doi.org/10.1016/j.exer.2006.08.004

Ishizawa, T., Saiura, A., & Kokudo, N. (2016). Clinical application of indocyanine green-fluorescence imaging during hepatectomy. *Hepatobiliary Surgery and Nutrition*, *5*(4), 322-328. doi:10.21037/hbsn.2015.10.01

Jafarnejad, M., Woodruff, M. C., Zawieja, D. C., Carroll, M. C., & Moore, J. E., Jr. (2015). Modeling lymph flow and fluid exchange with blood vessels in lymph nodes. *Lymphatic Research and Biology*, *13*(4), 234–247. https://doi.org/10.1089/lrb.2015.0028

Kim, J. H., & Caprioli, J. (2018). Intraocular pressure fluctuation: Is it important? *Journal of Ophthalmic & Vision Research*, *13*(2), 170–174. https://doi.org/10.4103/jovr.jovr_35_18

Kim, M., Johnston, M. G., Gupta, N., Moore, S., & Yucel, Y. H. (2011). A model to measure lymphatic drainage from the eye. *Experimental Eye Research*, *93*(5), 586–591. https://doi.org/10.1016/j.exer.2011.07.006

Kingman, S. (2004). Glaucoma is second leading cause of blindness globally. *Bulletin of the World Health Organization*, *82*(11), 887–888 doi: S0042-96862004001100019.

Morrison, J. C., Fraunfelder, F. W., Milne, S. T., & Moore, C. G. (1995). Limbal microvasculature of the rat eye. *Investigative Ophthalmology & Visual Science*, *36*(3), 751–756.

Morrison, J. C., Johnson, E. C., Cepurna, W. O., & Funk, R. H. (1999). Microvasculature of the rat optic nerve head. *Investigative Ophthalmology & Visual Science*, *40*(8), 1702–1709.

Negrini, D., & Moriondo, A. (2011). Lymphatic anatomy and biomechanics. *The Journal of Physiology*, *589*(Pt 12), 2927–2934. https://doi.org/10.1113/jphysiol.2011.206672

Nilsson, S. F., Sperber, G. O., & Bill, A. (1989). The effect of prostaglandin F2 alpha-1-isopropylester (PGF2 alpha-IE) on uveoscleral outflow. *Progress in Clinical and Biological Research*, *312*, 429–436.

Ninomiya, H., & Inomata, T. (2006). Microvasculature of the mouse eye: Scanning electron microscopy of vascular corrosion casts. *Journal of Experimental Animal Science*, *43*(3), 149–159 doi:10.1016j.jeas.2006.05.002.

Nur, I. H., & Güler, Ü. (2002). Histological investigations of the nictitating membrane (Palpebra Tertia III) in the New Zealand rabbit. *Fırat Üniversitesi Sağlık Bilimleri Dergisi*, *16*(2), 133–136.

Nur, I. H., Sacmaci, S., Keles, H., Abumandour, M., & Testereci, H. (2019). Application of quantum dot-based biosensor to the conjunctiva in Wistar albino rats. *Anatomia, Histologia, Embryologia*, *49*, 167–172. https://doi.org/10.1111/ahe.12508

Quigley, H. A., & Broman, A. T. (2006). The number of people with glaucoma worldwide in 2010 and 2020. *The British Journal of Ophthalmology*, *90*(3), 262–267. https://doi.org/10.1136/bjo.2005.081224

Raychaudhuri, U., Millar, J. C., & Clark, A. F. (2018). Knockout of tissue transglutaminase ameliorates TGF beta2-induced ocular hypertension: A novel therapeutic target for glaucoma? *Experimental Eye Research*, *171*, 106–110. https://doi.org/10.1016/j.exer.2018.03.009

Rosenblum, L. T., Kosaka, N., Mitsunaga, M., Choyke, P. L., & Kobayashi, H. (2011). Optimizing quantitative in vivo fluorescence imaging with near-infrared quantum dots. *Contrast Media & Molecular Imaging*, *6*(3), 148–152. https://doi.org/10.1002/cmmi.409

Schlotzer Schrehardt, U. (2007). MMPs in glaucoma. *Acta Ophthalmologica Scandinavica*, *85*(s240) doi: 10.1111/j.1600-0420.2007.01063_2981.x.

Swaminathan, S. S., Oh, D. J., Kang, M. H., & Rhee, D. J. (2014). Aqueous outflow: Segmental and distal flow. *Journal of Cataract and Refractive Surgery*, *40*(8), 1263–1272. https://doi.org/10.1016/j.jcrs.2014.06.020

Tam, A. L., Gupta, N., Zhang, Z., & Yucel, Y. H. (2011). Quantum dots trace lymphatic drainage from the mouse eye. *Nanotechnology*, *22*(42), 425101. https://doi.org/10.1088/0957-4484/22/42/425101

Tamm, E. R., Braunger, B. M., & Fuchshofer, R. (2015). Intraocular pressure and the mechanisms involved in resistance of the aqueous humor flow in the trabecular meshwork outflow pathways. *Progress in Molecular Biology and Translational Science*, *134*, 301–314. https://doi.org/10.1016/bs.pmbts.2015.06.007

Tham, Y. C., Li, X., Wong, T. Y., Quigley, H. A., Aung, T., & Cheng, C. Y. (2014). Global prevalence of glaucoma and projections of glaucoma burden through 2040: A systematic review and meta-analysis. *Ophthalmology*, *121*(11), 2081–2090. https://doi.org/10.1016/j.ophtha.2014.05.013

Toris, C. B., Camras, C. B., & Yablonski, M. E. (1993). Effects of PhXA41, a new prostaglandin F2 alpha analog, on aqueous humor dynamics in human eyes. *Ophthalmology*, *100*(9), 1297–1304. https://doi.org/10.1016/s0161-6420(93)31484-3

Toris, C. B., Risma, J. M., Gonzales-Martinez, J., McLaughlin, M. A., & Dawson, W. W. (2010). Aqueous humor dynamics in inbred rhesus monkeys with naturally occurring ocular hypertension. *Experimental Eye Research*, *91*(6), 860–865. https://doi.org/10.1016/j.exer.2010.09.011

Toris, C. B., Yablonski, M. E., Wang, Y. L., & Hayashi, M. (1995). Prostaglandin A2 increases uveoscleral outflow and trabecular outflow facility in the cat. *Experimental Eye Research*, *61*(6), 649–657. https://doi.org/10.1016/s0014-4835(05)80015-6

Varma, R., Lee, P. P., Goldberg, I., & Kotak, S. (2011). An assessment of the health and economic burdens of glaucoma. *American Journal of Ophthalmology*, *152*(4), 515–522. https://doi.org/10.1016/j.ajo.2011.06.004

Wong, T. Y., Loon, S. C., & Saw, S. M. (2006). The epidemiology of age related eye diseases in Asia. *British Journal of Ophthalmology*, *90*(4), 506–511. https://doi.org/10.1136/bjo.2005.083733

Yucel, Y., & Gupta, N. (2015). Lymphatic drainage from the eye: A new target for therapy. *Progress in Brain Research*, *220*, 185–198. https://doi.org/10.1016/bs.pbr.2015.07.028

Yucel, Y. H. (2010). Discovery of lymphatics in the human eye and implications. *Canadian Journal of Ophthalmology*, *45*(2), 115–117. https://doi.org/10.3129/i10-005

Yücel, Y. H., Johnston, M. G., Ly, T., Patel, M., Drake, B., Gümüş, E., … Gupta, N. (2009). Identification of lymphatics in the ciliary body of the human eye: A novel "uveolymphatic" outflow pathway. *Experimental Eye Research*, *89*(5), 810–819. https://doi.org/10.1016/j.exer.2009.08.0

How to cite this article: Nur İsmail Hakkı, Saçmacı Ş, Orhan İ, Perez W, Testereci H. Morphological analysis of aqueous humor drainage using QD nanoparticles and indocyanine green. *Microsc Res Tech*. 2020;83:1032–1044. https://doi.org/10.1002/jemt.23494